

Lithospheric and upper mantle structure of southern Tibet from a seismological passive source experiment

Xiaohui Yuan,^{1,2} James Ni,³ Rainer Kind,^{1,2} James Mechie,¹ and Eric Sandvol⁴

Abstract. Fifteen seismic stations were operated with about 20-km spacing in southern Tibet across the Zangbo suture (the collision zone between India and Asia) between May and October 1994 as part of the International Deep Profiling of Tibet and the Himalaya project (INDEPTH II) for wide-angle recording of the controlled source experiment and for passive earthquake recording. In addition, a dense deployment (4-km spacing) of stations within the German Depth Profiling of Tibet and the Himalayas (GEDEPTH) project also recorded a number of teleseismic earthquakes. The third data source used in this study is the records of the permanent broadband station at Lhasa. Teleseismic records have been obtained in sufficient quantity and quality to derive an image of the structure of the lithosphere and upper mantle from *P*-to-*S* converted phases. Important results are as follows. The Moho at 70–80 km and a second discontinuity at 50–60 km depth are observed over the entire profile south and north of the Zangbo suture. The data from the GEDEPTH dense array enable the detection of inclined structures penetrating the crust at the Zangbo suture. A pronounced low-velocity zone exists north of the Zangbo suture at about 10–20 km depth. The locations of the upper mantle discontinuities at 410 and 660 km depth are in agreement with the global reference model IASP91 [Kennett, 1991] over a large region of the Himalaya and southern Tibet.

1. Introduction

The International Deep Profiling of Tibet and the Himalaya (INDEPTH) project was started in 1992 with INDEPTH I and continued in 1994 with INDEPTH II. Within this project geoscientists from China, the United States, Germany and Canada are cooperating on questions of the lithospheric and upper mantle structures in Tibet. Results have been reported in a number of papers [Zhao *et al.*, 1993; Alsdorf *et al.*, 1996; Brown *et al.*, 1996; Makovsky *et al.*, 1996; Kind *et al.*, 1996; Chen *et al.*, 1996; Nelson *et al.*, 1996; Sandvol *et al.*, 1997]. Explosion seismic studies, studies of earthquake records, and magnetotelluric studies have been the main geophysical components of this project.

Kind *et al.* [1996] have reported about a first interpretation of the receiver functions observed along the INDEPTH II profile. An important result was the observation of a continuous Moho over the entire profile, south and north of the Zangbo suture zone. In contrast, in the seismic reflection section the Moho was only observed at the southern end of the INDEPTH I profile [Brown *et al.*, 1996]. A second important observation obtained by Kind *et al.* [1996] using receiver functions was the crustal low-velocity zone north of the Zangbo suture. This feature was correlated with other observations associated with the low-velocity zone, namely, “bright spots” seen in the seismic reflection profile [Brown *et al.*, 1996], strong

P-to-*S* conversions in the wide angle reflection sections [Makovsky *et al.*, 1996] and a high-conductivity layer in the magnetotelluric (MT) profile [Chen *et al.*, 1996].

The receiver function method [Owens *et al.*, 1984] was used by Kind *et al.* [1996] in its simplest form. This means all receiver functions at one station were summed and inverted for the *S* velocity structure of the crust. In this case the term “receiver function” means rotated and deconvolved seismic traces containing only (for flat layers) *P*-to-*S* converted energy at discontinuities underneath the station. The resulting *S* velocity models from neighboring stations are then compared for geological interpretation. Duecker and Sheehan [1997] have modified the receiver function method by summing traces with common conversion regions. In the present study we have applied another modification of the receiver function method. In the new version the individual traces are not summed but are used to produce images of the lithosphere and the entire upper mantle. These images are similar in appearance to reflection seismic images of the crust before migration. The new method produces a more detailed picture of the lithosphere and upper mantle than was previously possible.

Besides the improved method we also use more data than Kind *et al.* [1996]. We have added teleseismic recordings of the dense wide-angle German Depth Profiling of Tibet and the Himalayas (GEDEPTH) deployment, which proved to be very successful because of the close spacing of these stations. We have also added data from the permanent broadband station Lhasa (LSA), permitting a laterally extended view into the lithosphere and upper mantle.

The passive seismological part of INDEPTH II lasted from May until October 1994. Fifteen Reftek recording stations were operated in that time period. Nine stations were equipped with Guralp 3T broadband seismometers, and six with 1-Hz Mark L-4 seismometers. They were installed from the high Himalaya to approximately 150 km north of the

¹GeoForschungsZentrum Potsdam, Potsdam, Germany.

²Also at Freie Universität Berlin, Fachrichtung Geophysik, Berlin, Germany.

³Department of Physics, New Mexico State University, Las Cruces.

⁴Department of Geological Sciences, Cornell University, Ithaca, New York.

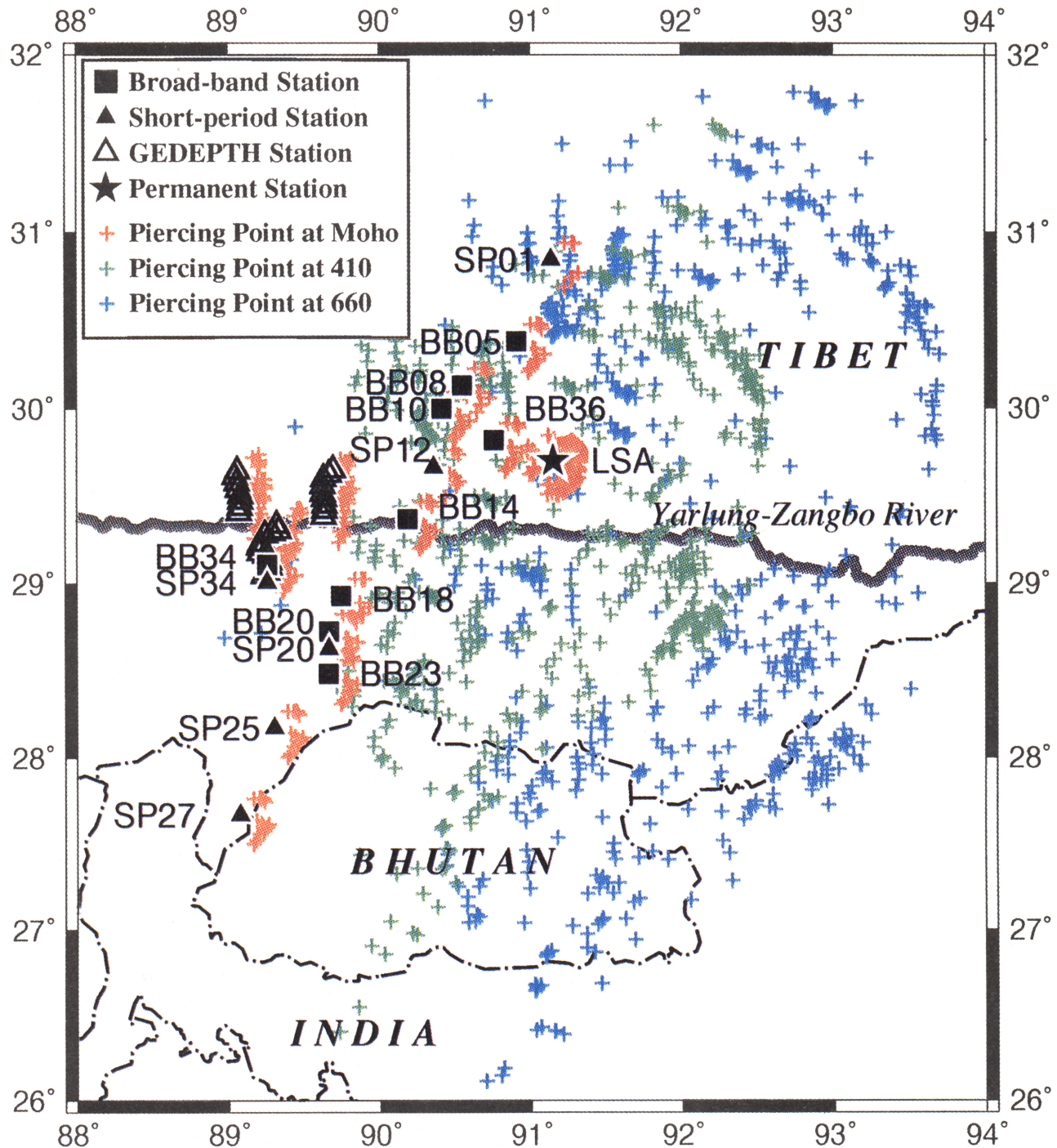


Plate 1. Location map of the broadband and short-period stations of the passive seismic experiment INDEPTH II, of the short-period GEDEPTH array and of the permanent broadband station LSA of the Chinese Digital Seismic Network. The Yarlung-Zangbo River marks the Zangbo suture. The locations of the conversion points for different depths are also shown for all teleseismic records used in this study.

Zangbo suture (Plate 1). The stations of the GEDEPTH deployment, the main purpose of which was the broadside wide-angle recording of the INDEPTH II shots, were also equipped with 1-Hz Mark L-4 seismometers.

2. Upper Mantle Discontinuities

Analyzing P -to- S converted waves in the coda of P is a standard method used in investigations of the upper mantle

discontinuities underneath a seismic station that was pioneered by Vinnik [1977]. Stammler *et al.* [1992] have applied this method to a number of globally distributed broadband stations. They detected clear P -to- S converted phases underneath practically all stations investigated. The differential travel times relative to P of the conversions from the 410- and 660-km discontinuities showed a correlation with surface geology. Stations on old shields had up to 4 s shorter travel times from both discontinuities than stations on tectonically younger

regions. This correlation is an indication that the upper mantle below old shields is cooler and faster than the upper mantle under younger regions. The differential travel times of the *P*-to-*S* conversions from both discontinuities do not vary by more than 2 s in continental regions. This led to the conclusion that the thickness of the upper mantle transition zone does not vary by more than about 20 km in continental regions. Subduction zones were not included in these data. *Gossler and Kind* [1996] found from a global analysis of *SS* precursors that the upper mantle transition zone underneath oceans is on the average about 14 km thinner than underneath continents. Accepting the hypothesis that petrological phase changes are the cause of both discontinuities, this observation was interpreted as being caused by a cooler transition zone underneath continents than underneath oceans. In this context it is very interesting to see if the Tibetan Plateau as the Earth's largest region with crustal doubling has any noticeable influence on the mantle transition zone at 410 and 660 km depth and also if the Tethyan slab has still noticeable effects beneath southern Eurasia [*van der Hilst et al.*, 1997].

About 40 events in the epicentral distance range from 35° to 85° with magnitudes greater than 5.6 were recorded in the observational period. Plate 1 shows a location map of the seismic broadband and short-period stations used for earthquake observations during the INDEPTH II project. Also shown are the locations of the short-period stations of the GEDEPTH experiment and the permanent broadband station at Lhasa (LSA) because their data have also been used. The locations of the conversion points (piercing points) of the incoming rays at the discontinuities at 660, 410, and 80 km depth are also marked in Plate 1. The original method of *Vinnik* [1977] used summation to identify weak converted signals from the upper mantle. We have modified this method and unified it with the receiver function method (if the latter is understood as a method to explore the crust) in a simple graphical presentation of all recorded seismic traces displaying converted *SV* energy from the upper crustal layers to the 660-km discontinuity. In the following, we describe the processing steps leading to this display (some steps are illustrated in Figure 1).

1. The response of the broadband or short-period instrument has been deconvolved from the original records (Figure 1b). This step makes it possible in many cases to broaden the response of short period instruments into a more useful teleseismic frequency band. With 24-bit resolution of the digital signal we had no problems restoring 20-s signals from magnitude 5.6 events. Restoring true ground motion from short period instruments helps in many cases where insufficient broad band instruments are available.

2. All traces have been rotated from the ZNE coordinate system into the LQT system. The LQT system is the ray coordinate system with L pointing in the ray direction. For a single ray in a flat, layered, and isotropic medium L, Q, and T contain only *P*, *SV*, and *SH* energy, respectively (Figure 1c). The eigenvalues of the covariance matrix are used for the computation of the rotation angles in a time window following the *P* arrival [e.g., *Kind et al.*, 1995]. The advantage of using the Q component instead of the radial component is the disappearance of projected *P* energy at the *P* arrival time. The first onset on the Q component is usually the *P*-to-*S* conversion from a discontinuity at some depth below the surface. It is therefore delayed with respect to the *P* onset.

3. We deconvolved the Q component with the *P* signal on the L component. This procedure makes different earthquake

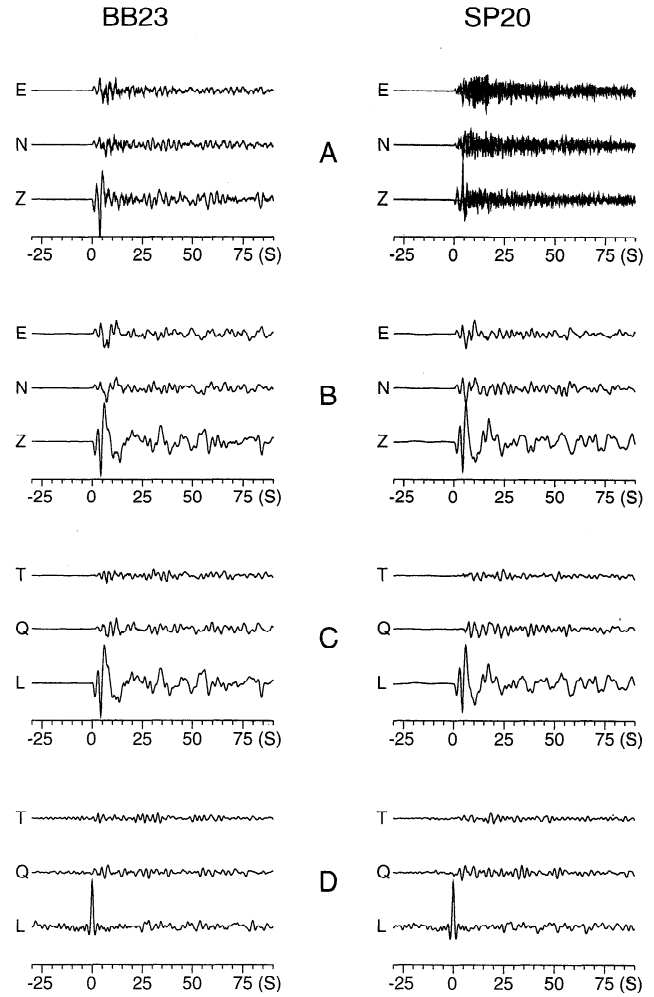


Figure 1. First steps of data processing for the receiver function analysis. (a) Examples of broadband (BB23) and short-period (SP20) original recordings, (b) after restoration of ground displacement, (c) after rotation from ZNE system to LQT system, and (d) after deconvolution.

records more comparable in their amplitudes and signal forms (see Figure 1d). Such a step has been used for many years in upper mantle conversion methods [*Vinnik*, 1977] and was also used in the first version of the receiver function method [*Phinney*, 1964]. The data have been filtered before deconvolution using a 3-pole, 2-s low pass filter.

4. We applied a distance moveout correction for *P*-to-*S* converted phases. This is a new, simple but very important step for conversions from the upper mantle. The converted phases in the coda of *P* originating at different depths have travel time curves which are not parallel to *P*. Their slowness decreases for increasing conversion depths. The distance moveout correction makes all these travel time curves parallel to the *P* curve, fixed at a certain epicentral distance. We have chosen 67° as the fixed distance. This means that the new corrected travel times are only valid for this distance. Timescales of seismograms from larger distances are stretched, while timescales from shorter distances are compressed. This is very similar to the distance moveout correction in seismic reflection processing. This procedure therefore produces very similar images to seismic reflection images. It is thus possible to display conversions from all depths in a single figure with all conversions parallel to

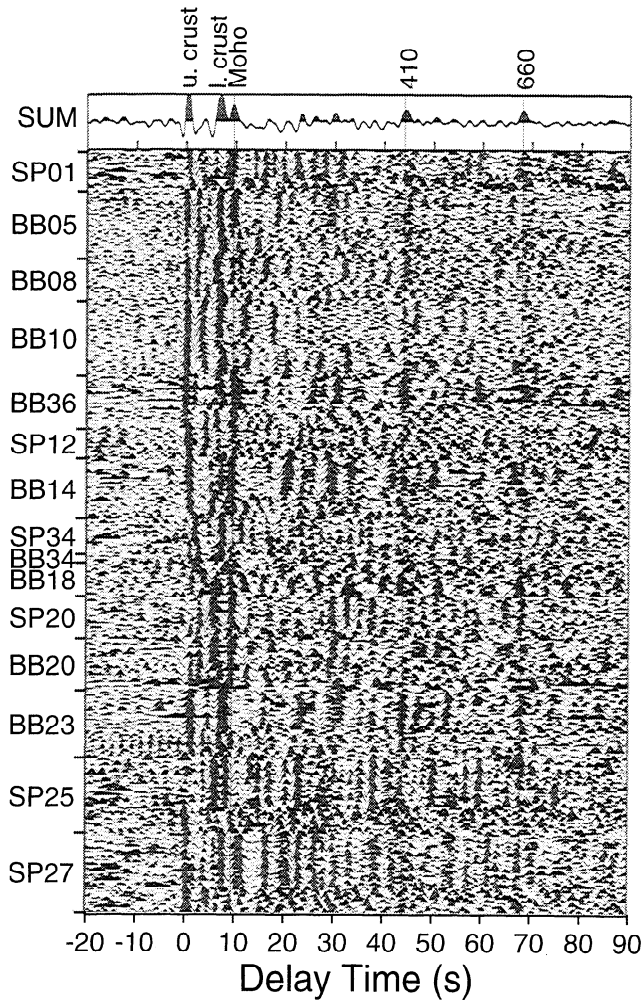


Figure 2. Plot of all recorded receiver functions of the passive source INDEPTH II deployment. The traces are plotted equally spaced and are distance moveout corrected for P -to- S converted waves underneath the stations. The timescale is valid for 67° epicentral distance. Several crustal and upper mantle phases can be clearly recognized (especially in the summation trace on top). The lines at the 410- and 660-km conversions belong to the IASP91 global reference model. The line at the Moho is plotted through the peak of the summed Moho phase.

P , provided the layering is flat. Multiples will not be parallel to P if the traces are sorted by epicentral distance. The wave forms are however slightly distorted after this procedure. The IASP91 model was used to compute the distance moveout corrections.

All 340 processed traces are plotted equally spaced in Figure 2. They are ordered first according to station and second according to the backazimuth running clockwise from north at the top. As most events are from the northeast and southeast, this also means an approximate ordering of the events according to latitude. The summation trace of all 340 traces is also displayed. The timescale is the delay time with respect to the P phase at 67° . All traces are normalized individually. In the first 10 s we see only crustal effects. The main phases consistent over the entire profile are labeled at the summation trace. They are signals from an upper crustal discontinuity at about 2 s, from the lower crust at about 7 s, and from the Moho at

about 10 s. From the upper mantle we see signals from the 410- and 660-km discontinuities. No clear signal is visible between the Moho and 410 km. The conversions from 410 and 660 km depth are recognizable signals over the entire profile, and their summation is a very clear signal. The two thin lines plotted at both mantle signals are the theoretical travel times of the IASP91 reference Earth model.

Close to the INDEPTH II profile is the permanent broadband station of the Chinese Digital Seismic Network (CDSN) at Lhasa (LSA). Data from this station have been processed in the same way as from the stations of the temporary INDEPTH II profile. The results from about 210 earthquake records are shown in Plate 2. The receiver functions are plotted equally spaced as a function of the backazimuth. The backazimuth and epicentral distance of each trace are indicated on the right of Plate 2. The Moho at 10 s is visible over the entire circular profile, in addition to an upper crustal layer at 2 s and a lower crustal layer at 7–8 s. These crustal phases seem identical with those observed in the summation trace of the INDEPTH stations. The upper mantle discontinuities at 410 and 660 km depth are again visible. The 410 km discontinuity seems to have more scatter at LSA than at INDEPTH II and the 660-km discontinuity seems to be weaker. In addition, there are a few more upper mantle discontinuities visible. The clearest ones are at about 280, 380, and 520 km depth. We have also plotted the LSA data as a function of the epicentral distance and found no indication that the 280-, 380-, and 520-km discontinuities have a slowness different to that of a P -to- S conversion. This means they are probably not multiples. There might be a weak indication of a slight dip of the discontinuities between the Moho and the 410-km discontinuity toward the northeast (0 to 90° backazimuth). We have also looked at the transverse component of the LSA data, which could indicate dipping structures [Zhu et al., 1995]. The largest amplitudes on the transverse component are seen later than 10 s, which could be evidence for dipping structures below the crust. Indications for dipping layers in the crust are weak at LSA, and they do not exist for the 410- and 660-km discontinuities. Since station LSA has been running for many years, it has recorded much more data than the INDEPTH II project. Therefore better quality data could be selected which leads to a better resolution of the additional upper mantle discontinuities. The causes of these additional upper mantle discontinuities could be petrological phase changes or changes in composition. Since we only have information about these discontinuities underneath one station, it is too early to speculate about their role in the dynamics of the Tibetan Plateau.

The conversion times from the 660-km discontinuity for IASP91, INDEPTH II and LSA are 68.1, 68.2 and 68.0 s, respectively. The travel times of Stammler et al. [1992] for other stations of the CDSN outside Tibet vary between 68.1 and 68.8 s. All these travel times are in sufficient agreement considering that the scatter of the data used for summation seems to be close to 1 s. The depth of the 660-km discontinuity in southern Tibet can be considered constant and in good agreement with IASP91. The conversion times from the 410-km discontinuity for IASP91, INDEPTH II, and LSA are 44.1, 44.4, and 43.4 s, respectively. The INDEPTH II time is in good agreement with the IASP91 time, whereas the LSA time is one second less than the INDEPTH II time. Stammler et al. [1992] have times between 44.1 and 44.7 s for the stations of the CDSN outside Tibet. A closer look at the 410-km discontinuity at LSA shows that this phase is complicated. It seems to have

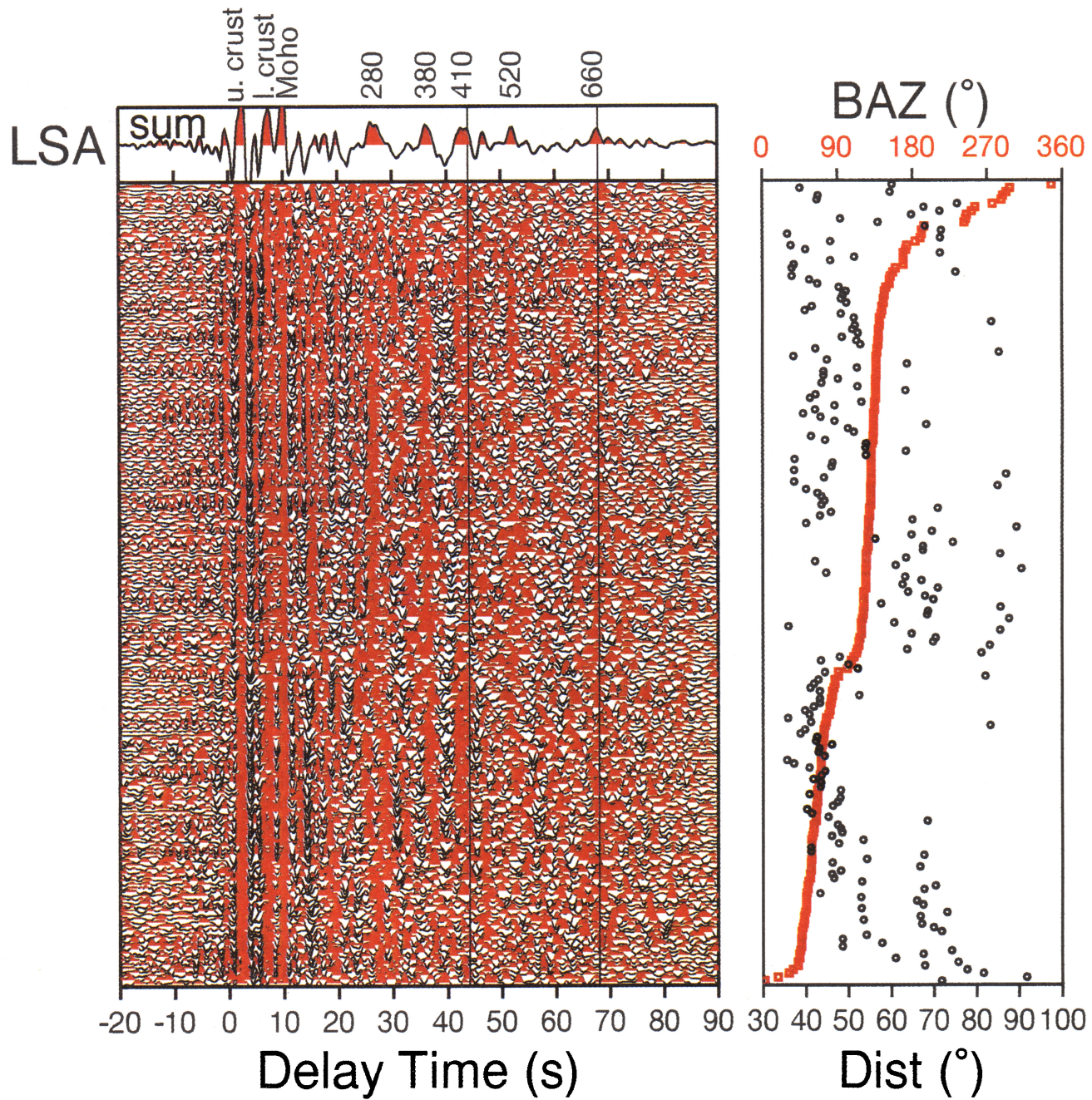


Plate 2. Receiver functions of the permanent broadband station LSA of the Chinese Digital Seismic Network at Lhasa. The traces are plotted equally spaced and the backazimuth and epicentral distance of each trace are shown on the right. The summation of all traces is shown at the top. The same crustal phases as in the INDEPTH II data in Figure 2 can be seen. Also the upper mantle phases at 410 and 660 km depth are visible, in addition to a number of additional upper mantle phases.

a more complicated waveform that could be an indication of a complex or distorted 410-km discontinuity under LSA. Duecker and Sheehan [1997] found a surprisingly large topography (20–30 km or about 3 s) of both upper mantle discontinuities across the Yellowstone hotspot track.

Plate 1 shows that the conversion points in the upper mantle cover a region of about 600×400 km of the Himalaya and southern Tibet. No difference to the global average model was found for the major part of this region. Only in the eastern part of the region (at LSA) the discontinuity at 410 km seems to be

anomalous. It appears about 10 km shallower, which would indicate a cooler temperature because of the positive Clapeyron slope of the phase transformation curve in the PT diagram. We speculate that this anomaly is related to the old Tethyan slab found by van der Hilst *et al.* [1997] in the lower mantle.

Most authors regard the upper mantle discontinuities as sharp. This is mainly based on observations of high frequency precursors of $P'P'$ by Benz and Vidale [1993]. Petersen *et al.* [1993], however, argued in favor of a less sharp 660-km discontinuity. Their results were based on the width of the P -to- S

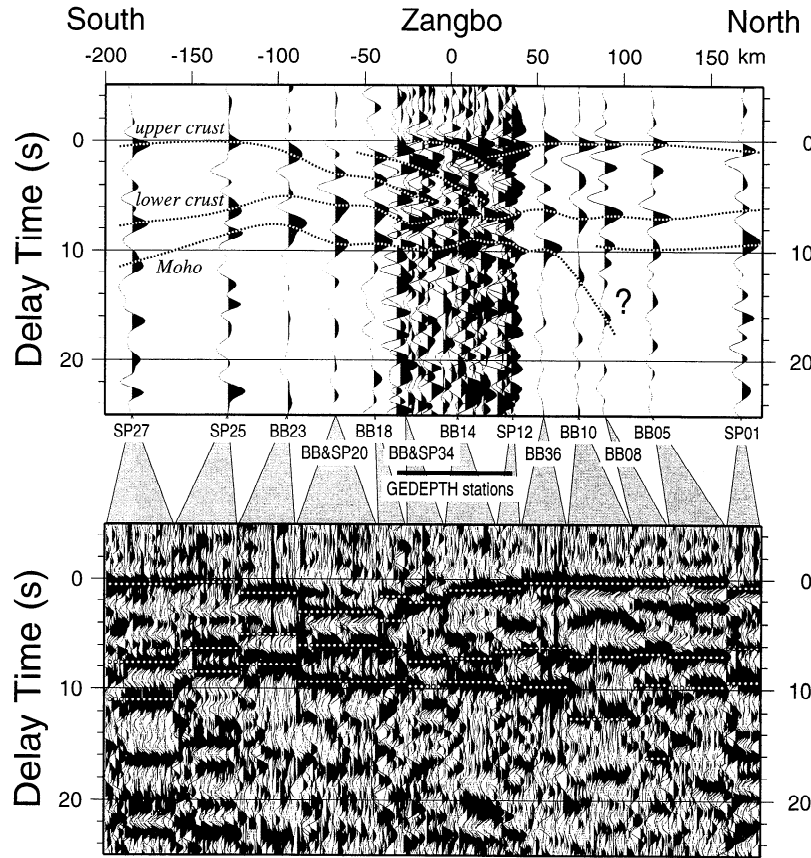


Figure 3. (bottom) First 25 s of the receiver functions of the INDEPTH II data from Figure 2. The phases labeled in the summation trace in Figure 2 are marked for each station. (top) INDEPTH II and GEDEPTH teleseismic data plotted according to the distance of their Moho piercing points from the Zangbo suture. The traces of each station have been summed. The same correlations are marked as in the bottom part of the figure. More details can be seen at the Zangbo suture because of the densely spaced GEDEPTH stations. Note indications of structures penetrating the crust at the Zangbo suture. There are also indications of complications in the structure of the Moho north of the Zangbo suture.

converted signals that used summed traces as suggested by Vinnik [1977]. Our observations in Figure 2 and Plate 2, however, suggest that for any interpretation of signal form data, individual traces should be used and not summed traces. Scatter of the data in the range of 1 s cannot be excluded in the summed traces. This makes any interpretation of the width of the summed traces questionable. Moreover, in some regions where the 220-km discontinuity exists, multiples of the “220” interfere with P -to- S conversions from the 660-km discontinuity [Bostock, 1996]. Although these multiples have a different slowness, if we sum along the P -to- S moveout curve of the 660-km discontinuity, these multiples will broaden the waveform of the P 660S summation trace.

3. Crustal Receiver Function Analysis

Figure 3 (bottom) shows the first 25 s of the receiver functions in Figure 2. The phases labeled in the summation trace of Figure 2 are also marked at each station in the bottom part of Figure 3. The same data are plotted in Figure 3 (top) with all data summed at each station. In addition to the INDEPTH II data the teleseismic records of the GEDEPTH project are also plotted in Figure 3. The data are plotted according to the distance of the stations from the Zangbo suture. The dotted lines labeled “upper crust,” “lower crust,” and “Moho” are

phases identified in Figure 2 and Figure 3 (bottom). The trace spacing in Figure 3 (bottom) has the advantage of making phase correlations easier but it has the disadvantage of a varying distance scale. The distance spacing in Figure 3 (top) has the advantage of being a linear distance scale, but the disadvantage of making lateral correlations more difficult if there are gaps in the profile. Both types of images should therefore always be considered together. The closely spaced GEDEPTH stations are located north and south of the Zangbo suture and permit a very detailed view of the crustal structure there. It seems as if there are inclined structures penetrating nearly the entire crust. This observation could coincide with observations of north dipping reflections in the INDEPTH common midpoint (CMP) profile at the same location [Nelson et al., 1996]. The phase labeled “upper crust” starts at the southern end of the profile dipping gently to the north. It should be remembered that because of the use of the Q component instead of the R component there is no energy at zero arrival time if there is no discontinuity close to the surface. The phase labeled “lower crust” seems to be continuous over the entire profile. There appears to be a downbending of the Moho at stations BB36 and BB10, but the station spacing is too large for a clear observation. The general picture of the complicated undulating or faulted structure of the Moho seems to be in agreement with

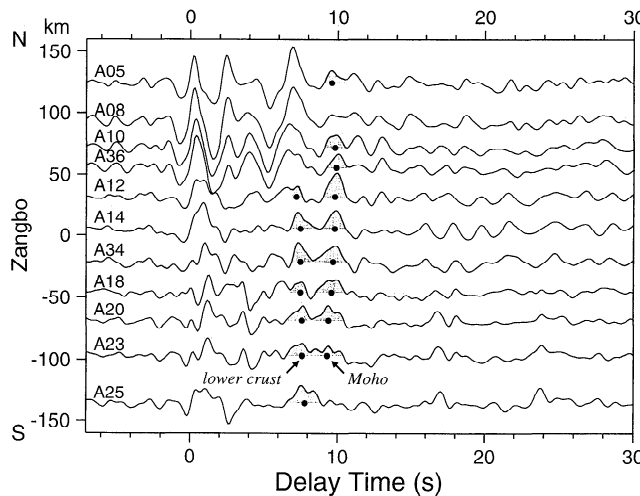


Figure 4. Q components as in Figure 2 except for the fact that in this case each trace is the result of summation of the traces from three neighboring stations (for example, A05 contains the traces from the stations SP01, BB05, and BB08). Lower crustal phase and Moho are marked.

the observations of Hirn *et al.* [1984]. Zhu and Helmberger [1996] have observed an earthquake hypocenter below the crust at the Zangbo suture from which they conclude low upper mantle temperatures.

To improve the coherency between stations for the inversion of the receiver functions, we have applied a spatial low-pass filter. This was achieved by taking the moving average over three neighboring stations. The result is shown in Figure 4. The trace A05 in Figure 4 results from averaging the Q traces from the stations SP01, BB05, and BB08; trace A08 is the average of BB05, BB08, and BB10; and so on. The spatially filtered receiver functions in Figure 4 are the input data for our inversion. The Moho is not very clear north of 50 km from the Zangbo suture in the spatially filtered traces. This could be caused by a very heterogeneous Moho in this region as can be seen in the single traces image in Figure 3 (bottom), or the Moho P-to-S conversion contains interference from multiples from the crustal low-velocity zone. The northernmost traces, A36 to A05, have very strong energy between 0 and 8 s. These strong amplitudes are the dominating feature in the filtered traces north of the Zangbo suture in Figure 4.

The inversion method used is described by Kind *et al.* [1995]. Plane wave theoretical seismograms are computed for the starting model using the method of Haskell [1962] for an angle of incidence averaged over all epicentral distances. The theoretical traces are rotated and deconvolved in the same manner as the observed traces. The optimal parameters of the model are found by iteratively minimizing the mean square deviation of the observed and theoretical traces and of the starting and final models [Kind *et al.*, 1995]. The results of the inversions are shown in Figures 5 and 6. The thin line in the model on the left side of Figure 5 (A05) represents the starting model, and the heavy line represents the final model. Adjacent to the model in Figure 5 (A05) the dashed line represents the data, the thin line belongs to the starting model, and the thick line belongs to the final model. The top trace on the right of Figure 5 (A05) is the deconvolved P signal of the L component with its amplitude normalized to one. The amplitude scale of the Q component is marked and is different from the amplitude scale of the

P signal. The starting model is a shear velocity model. The P velocity was fixed with a Poisson's ratio of 0.25 [Rodgers and Schwartz, 1997; Owens and Zandt, 1997], and the density was fixed by Birch's law [Birch, 1961]. The fit between the theoretical seismograms of the final model and the data seems reasonable. In Figure 5 the inversion of the LSA receiver functions is also shown.

Figure 7 summarizes all resulting models. The models derived from the receiver functions A05, A08, A10, and A36 are all very similar. Their main feature is a pronounced low-velocity zone at about 15–20 km depth. A shallower upper crust low-velocity zone is also observed at the permanent station LSA, which is located about 50 km to the east of station BB36. Zhao *et al.* [1996] have also derived shear velocity models from LSA receiver functions and the stations of the 1991–1992 Program for Array Seismic Studies of the Continental Lithosphere (PASSCAL) Tibet deployment. They did not observe the low-velocity zone at LSA and at neighboring stations in southern Tibet. This is probably due to their data being mostly of longer period, which could not resolve this structure. Between stations SP25 and BB36 a lower crustal discontinuity between 50 and 60 km depth is obtained from our receiver function analysis and was also observed in Zhao *et al.*'s. [1996] receiver function analysis of the LSA data and data from neighboring stations. Deeper structure does not show up in the traces A05, A08, and A10. For these traces the Moho and the lower crustal discontinuity are not obtained in the inversion. This does not mean that they do not exist there. The Moho is observed in Figure 3 (bottom) at stations SP01 and BB05, it is poor at station BB08, and it is observed at BB10 but deeper. At BB36 the Moho is again observed and is also seen in the filtered receiver function A36. The Moho is laterally highly variable north of 50 km from the Zangbo suture and is therefore suppressed in the summed (meaning laterally low-pass filtered) traces used for the model computations in Figures 5–7. Effects of the lower crustal discontinuity and of reverberations in the low velocity zone cannot be separated in Figure 4. It seems as if the reverberation effects are stronger since the general amplitude level is much higher at traces A36, A10, A08, and A05, where a low-velocity zone is obtained.

The applied inversion method is not unique, since it tries by definition to find models close to the starting model. The method may be successful for different pairs of starting and final models, meaning the final model depends on the choice of a physically reasonable starting model. We did this by choosing the simplest starting model and then adding a priori information [Ammon *et al.*, 1990] we saw in the data, such as conversions from the Moho or the lower crust. The role of the numerical inversion is merely to improve the fit of the data. However, it should be noted that at the northernmost stations we did not include a low-velocity zone in the starting model. At these stations the inversion produced a significant change in the starting model by adding a pronounced low-velocity zone in the crust.

4. Discussion

The results of the receiver function analysis of the INDEPTH II, LSA, and GEDEPTH recordings are shown in Figures 2, 3, and 7 and Plate 2. The receiver functions are analyzed in two different ways. First, individual traces are presented in images permitting lateral correlation of phases, as in reflection seismic images (Figures 2 and 3 and Plate 2). The

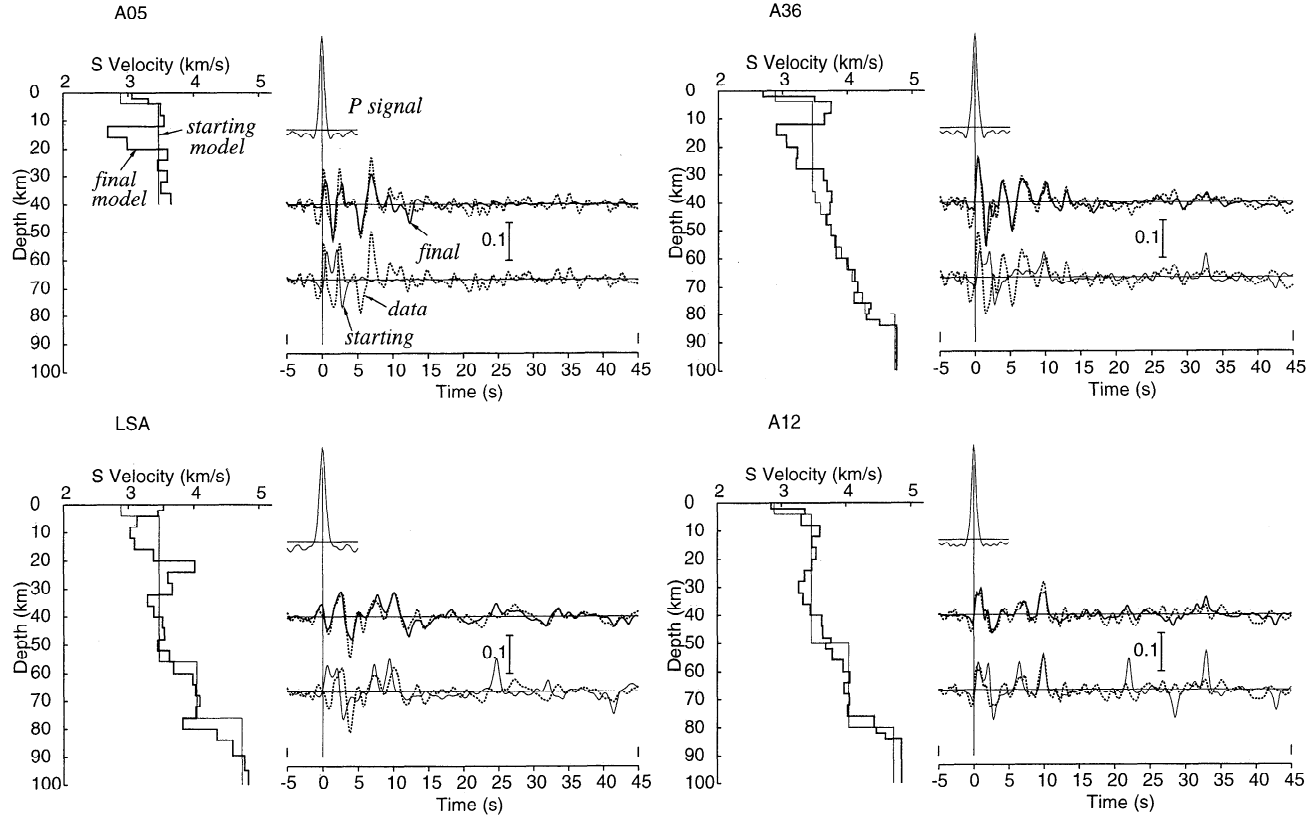


Figure 5. Inversion of averaged receiver functions of the INDEPTH II stations and of the permanent broadband station LSA. Starting and final models are shown by thin and thick lines in the left half of each results panel, respectively. The dashed line in the right of each panel is the observed receiver function, the thin line is the theoretical receiver function belonging to the starting model, and the thick line belongs to the final model. The top trace on the right is the input P signal, which has the normalized amplitude 1. The amplitude scale of the Q components is shown. The converted waves are about 10% of the input signal.

results of this analysis are Moho observations between 70 and 80 km depth along the entire profile; observations of inclined structures penetrating the crust and disturbing the Moho 50 km north of the Zangbo suture; observations of the 410- and 660-km upper mantle discontinuities at their global average positions with a complication of the 410-km discontinuity observed at LSA. In the CMP reflection data the Moho was only observed at the south end of the INDEPTH I profile at a depth of 75 km [Brown et al., 1996]. In Figure 2 the Moho can be identified over nearly the entire profile, and it is also seen clearly at the same depth at LSA. Hirn et al. [1984] observed Moho jumps of 10–15 km in southern Tibet with wide-angle reflection fan profiling. We have indications between stations BB36 and BB05 (see Figures 2 and 3) for a Moho undulation of about the same size, where the inclined structures of the Zangbo suture arc also observed. This could be a confirmation of the observation by Hirn et al. [1984]. However, the spacing of the INDEPTH II earthquake stations is too large to show enough details. A station spacing as in the GEDEPTH deployment (4 km) would be required farther north for higher resolution. Therefore it is still difficult to interpret the significance of the apparent mantle imbrication associated with the Zangbo suture. The Indian lower lithosphere is considered to under-thrust the Asian crust to the Banggong suture [Ni and Barazangi, 1983; Beghoul et al., 1993; Owens and Zandt, 1997], which is beyond the present INDEPTH transect.

Brown et al. [1996] observed a steeply north dipping reflector in the lower crust between the broadband stations BB14 and BB36. The receiver functions in Figure 3 also indicate north dipping structures at this location. Brown et al. [1996] also observed reflections from the Main Himalayan thrust (MHT) fault at 30–40 km depth near the stations BB23 and BB20 at the southern end of the INDEPTH II profile. We also see a phase parallel to the MHT but shallower, labeled “upper crust.” This phase can be followed from the southern end of the profile dipping gently north to the Zangbo suture. The fact that these two discontinuities are observed at different depths could be caused by the different frequencies used in the reflection and receiver function techniques.

The second method applied to analyze the receiver functions is the common method of inversion into a velocity-depth distribution. This inversion derives information about physical crustal properties from amplitude information in seismograms. Since amplitudes are often not very stable, many individual traces from several stations have been summed to obtain improved lateral consistency. The estimated crustal and mantle P and S velocities (Figures 5 and 6) are in good agreement with the observations by Rodgers and Schwartz [1997]. The most important result of this inversion is the identification of a pronounced low-velocity zone between about 10 and 20 km depth north of the Zangbo suture [Kind et al., 1996]. This zone is also observed at station LSA about 50 km southeast of the

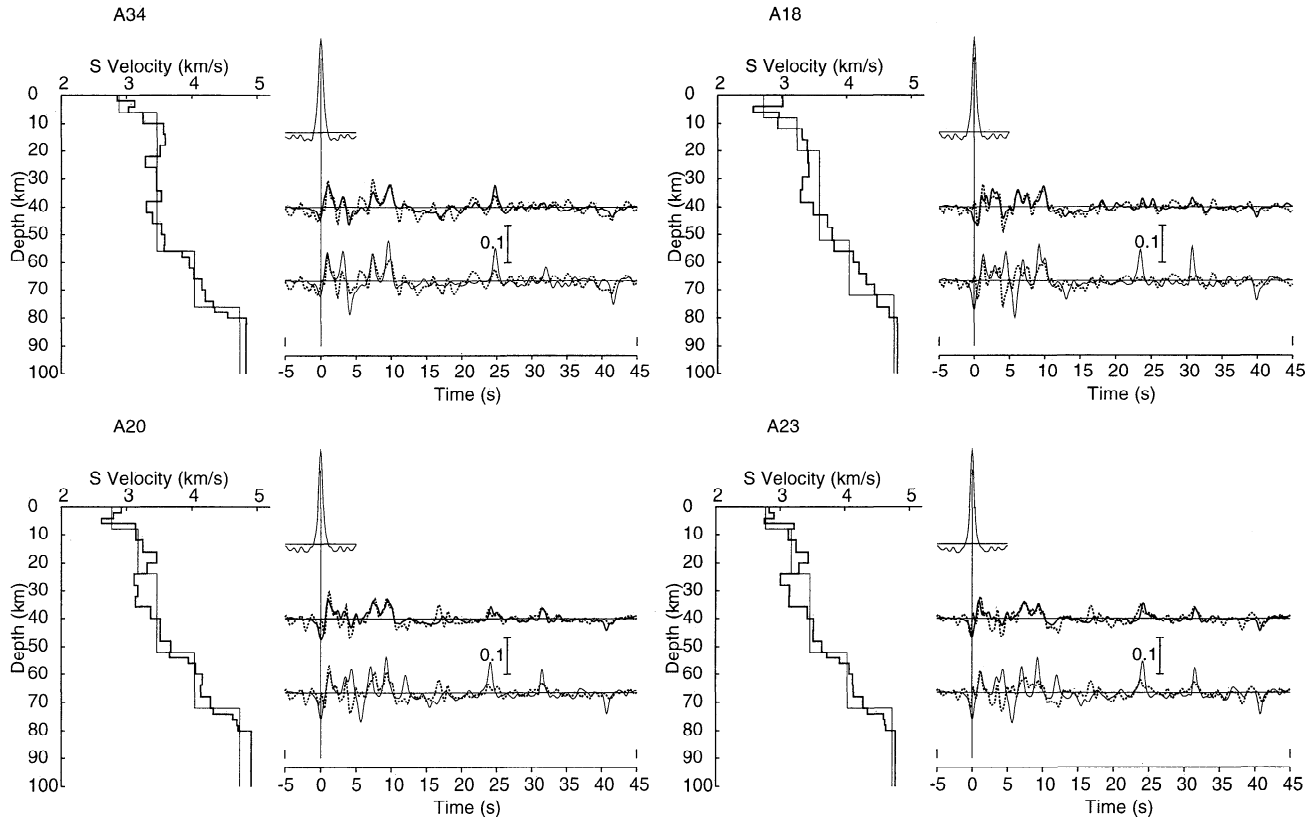


Figure 6. More examples of receiver function inversions of INDEPTH II stations.

profile. Evidence of the low-velocity zone has also been obtained using wide and steep angle controlled source methods within the INDEPTH project [Makovsky et al., 1996; Brown et al., 1996]. It is interpreted as being caused by partial melt [Nelson et al., 1996] in agreement with the geodynamic model of Zhao and Morgan [1987].

Another very interesting observation is the phase labeled “lower crust” in Figures 2, 3, and 4 and Plate 2. It appears at a depth of 50–60 km (6–8 s differential time) underneath practically the entire area. It is also seen in the S velocity models obtained from the receiver functions in Figure 7 at an average depth of 55 km. This discontinuity appears also in the

model of Owens and Zandt [1997] in which they interpreted the layer below this discontinuity as part of the underthrust Indian lower crust.

Acknowledgments. We wish to thank Wenjin Zhao, Kefen Wu, Manfred Brunner, Axel Fabritius, and John Nabelek for their support and cooperation. We also wish to thank Günter Bock for critically reading the manuscript and George Zandt, Ken Duecker, and an anonymous reviewer for their helpful reviews, which have contributed much to the improvement of this paper. Some of the figures have been generated using the Generic Mapping Tool [Wessel and Smith, 1991]. Xiaohui Yuan was supported by the Deutsche Akademische Austausch-

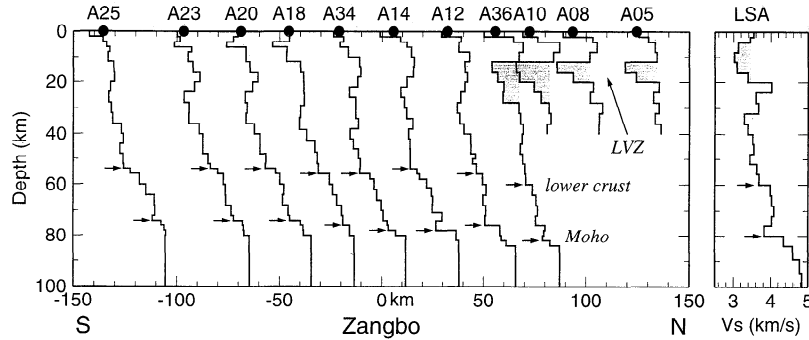


Figure 7. Summary of southern Tibet crustal models observed at the INDEPTH II stations and at LSA. Prominent features include the crustal low velocity zone north of the Zangbo suture, also observed at LSA. The Moho is observed over most of the profile between 70 and 80 km depth. At stations BB05 and BB10 the Moho can be observed in Figure 2. The lower crust discontinuity at about 55 km depth is widespread in the region.

chdienst (DAAD) and the Deutsche Forschungsgemeinschaft. This research was partially funded by the National Science Foundation grant NSF EAR-9316814. The wide-angle array GEDEPTH was funded by the Deutsche Forschungsgemeinschaft.

References

- Alsdorf, D., L. Brown, and D. Nelson, Possible upper mantle reflection fabric on seismic profiles from the Tethyan Himalaya: Identification and tectonic interpretation, *J. Geophys. Res.*, 101, 25,305–25,320, 1996.
- Ammon, C. J., G. E. Randall, and G. Zandt, On the nonuniqueness of receiver function inversions, *J. Geophys. Res.*, 95, 15,303–15,318, 1990.
- Beghoul, N., M. Barazangi, and B. L. Isacks, Lithospheric structure of Tibet and western north America: Mechanisms of uplift and a comparative study, *J. Geophys. Res.*, 98, 1997–2016, 1993.
- Benz, H. M., and J. E. Vidale, Sharpness of upper mantle discontinuities determined from high frequency reflections, *Nature*, 365, 147–150, 1993.
- Birch, F., The velocity of compressional waves in rocks to 10 kilobars, 2, *J. Geophys. Res.*, 66, 2199–2224, 1961.
- Bostock, M. G., A seismic image of the upper mantle beneath the North American Craton, *Geophys. Res. Lett.*, 23, 1593–1596, 1996.
- Brown, L. D., W. Zhao, K. D. Nelson, M. Hauck, D. Alsdorf, A. Ross, M. Cogan, M. Clark, X. Liu, and J. Chen, Bright spots, structure, and magmatism in southern Tibet from INDEPTH seismic reflection profiling, *Science*, 274, 1688–1690, 1996.
- Chen, L., J. R. Booker, A. G. Jones, N. Wu, M. J. Unsworth, W. Wenbo, and H. Tan, Electrically conductive crust in southern Tibet from INDEPTH magnetotelluric surveying, *Science*, 274, 1694–1696, 1996.
- Duecker, K. G., and A. F. Sheehan, Mantle discontinuity structure from midpoint stacks of converted P to S waves across the Yellowstone hotspot track, *J. Geophys. Res.*, 102, 8313–8327, 1997.
- Gossler, J., and R. Kind, Seismic evidence for very deep roots of continents, *Earth Planet. Sci. Lett.*, 138, 1–13, 1996.
- Haskell, N. A., Crustal reflections of plane P and SV waves, *J. Geophys. Res.*, 67, 4751–4767, 1962.
- Hirn, A., et al., Crustal structure and variability of the Himalaya border of Tibet, *Nature*, 307, 23–25, 1984.
- Kennett, B. L. N., *IASPEI 1991 Seismological Tables*, 167 pp., Res. Sch. of Earth Sci., Aust. Natl. Univ., Canberra, Australia, 1991.
- Kind, R., G. L. Kosarev, and N. V. Petersen, Receiver functions of the stations of the German regional Seismic Network (GRSN), *Geophys. J. Int.*, 121, 191–202, 1995.
- Kind, R., J. Ni, W. Zhao, J. Wu, X. Yuan, L. Zhao, E. Sandvol, C. Reese, J. Nabelek, and T. Hearn, Evidence from earthquake data for a partially molten crustal layer in southern Tibet, *Science*, 274, 1692–1694, 1996.
- Makovskiy, Y., S. L. Klempner, L. Ratschbacher, L. D. Brown, M. Li, W. Zhao, and F. Meng, INDEPTH wide-angle reflection observation of P -wave-to- S -wave conversion from crustal bright spots in Tibet, *Science*, 274, 1690–1691, 1996.
- Nelson, K. D., et al., Partially molten middle crust beneath southern Tibet: Synthesis of project INDEPTH results, *Science*, 274, 1684–1688, 1996.
- Ni, J., and M. Barazangi, High-frequency seismic wave propagation beneath the Indian Shield, Himalayan Arc, Tibetan Plateau and surrounding regions: High uppermost mantle velocities and efficient S_n propagation beneath Tibet, *Geophys. J. R. Astron. Soc.*, 72, 665–689, 1983.
- Owens, T. J., and G. Zandt, Implications of crustal property variations for models of Tibetan plateau evolution, *Nature*, 387, 37–43, 1997.
- Owens, T. J., G. Zandt, and S. R. Taylor, Seismic evidence for an ancient rift beneath the Cumberland Plateau, Tennessee: A detailed analysis of broadband teleseismic P waveforms, *J. Geophys. Res.*, 89, 7783–7795, 1984.
- Petersen, N., L. Vinnik, G. Kosarev, R. Kind, S. Oreshin, and K. Stammle, Sharpness of mantle discontinuities, *Geophys. Res. Lett.*, 20, 859–862, 1993.
- Phinney, R. A., Structure of the Earth's crust from spectral behavior of long-period body waves, *J. Geophys. Res.*, 69, 2997–3017, 1964.
- Rodgers, A., and S. Y. Schwartz, Low crustal velocities and mantle lithospheric variations in southern Tibet from regional P_n waveforms, *Geophys. Res. Lett.*, 24, 9–12, 1997.
- Sandvol, E., J. Ni, R. Kind, and W. Zhao, Seismic anisotropy beneath the southern Himalayas–Tibet collision zone, *J. Geophys. Res.*, 102, 17,813–17,823, 1997.
- Stammle, K., R. Kind, N. Petersen, G. Kosarev, L. Vinnik, and Q. Liu, The upper mantle discontinuities: Correlated or anticorrelated? *Geophys. Res. Lett.*, 19, 1563–1566, 1992.
- van der Hilst, R. D., S. Widjiantoro, and E. R. Engdahl, Evidence for deep mantle circulation from global tomography, *Nature*, 386, 578–584, 1997.
- Vinnik, L. P., Detection of waves converted from P to SV in the mantle, *Phys. Earth Planet. Inter.*, 15, 294–303, 1977.
- Wessel, P., and W. H. F. Smith, Free software helps map and display data, *Eos Trans. AGU*, 72, 441, 445–446, 1991.
- Zhao, L. S., M. K. Sen, P. Stoffa, and C. Frohlich, Application of a very fast simulated annealing to the determination of the crustal structure beneath Tibet, *Geophys. J. Int.*, 125, 355–370, 1996.
- Zhao, W., and J. Morgan, Injection of Indian crust into Tibetan lower crust: A two-dimensional finite element model study, *Tectonics*, 6, 489–504, 1987.
- Zhao, W., K. D. Nelson, and Project INDEPTH Team, Deep seismic reflection evidence for continental underthrusting beneath southern Tibet, *Nature*, 366, 557–559, 1993.
- Zhu, L., and D. Helmberger, Intermediate depth earthquakes beneath the India-Tibet collision zone, *Geophys. Res. Lett.*, 23, 435–438, 1996.
- Zhu, L., T. J. Owens, and G. E. Randall, Lateral variation in crustal structure of the northern Tibetan Plateau inferred from teleseismic receiver functions, *Bull. Seismol. Soc. Am.*, 85, 1521–1540, 1995.
-
- R. Kind, J. Mechle, and X. Yuan, GeoforschungsZentrum Potsdam, Telegrafenberg, 14473 Potsdam, Germany. (e-mail: kind@gfz-potsdam.de)
- J. Ni, Department of Physics, New Mexico State University, Las Cruces, NM 88003.
- E. Sandvol, Department of Geological Sciences, Cornell University, Ithaca, NY 14853.

(Received September 10, 1996; revised June 7, 1997;
accepted August 20, 1997.)